Superconductivity and spin-density waves

L. L. Daemen and A. W. Overhauser
Department of Physics, Purdue University, West Lafayette, Indiana 47907
(Received 23 November 1988)

Superconductivity in a metal with a spin-density-wave (SDW) broken symmetry is investigated within the framework of the Bardeen-Cooper-Schrieffer (BCS) theory. The gap equation is solved analytically leading to a gap that falls to zero at the SDW gap for a spiral SDW, and to a small, but nonzero value, for a linear SDW. The electronic specific heat in the superconducting state acquires a low-temperature tail, far in excess of a BCS exponential falloff. The ultrasonic attenuation exhibits a similar deviation from the usual BCS result.

I. INTRODUCTION

Baltensperger and Strässler[1] proved some 25 years ago that superconductivity and antiferromagnetism are compatible. Recently, Nass *et al.*[2] investigated the problem of superconductivity in the presence of a spin-density wave (SDW) for Chevrel compounds, and Psaltakis and Fenton[3] have studied the influence of SDW's in a one-dimensional organic superconductor. In this paper we examine superconductivity in a SDW metal, for which the SDW is a high-temperature phenomenon (i.e., $G \gg \Delta$, where $2G$ is the SDW energy gap). The motivation for this study is twofold; first, it is complementary to prior work[1,2,3] and second, the results obtained suggest a possible resolution of the longstanding problem in the specific heat of superconducting Pb.

Twenty-five years ago, Keesom and van der Hoeven[4,5] discovered that the specific heat of lead in the superconducting state exhibits an unexpected low-temperature tail shown in Fig. 1. It has been argued that such behavior, observed in the heavy-fermion compound UBe_{13},[6] is indicative of exotic pairing. However, Pb is a spin-singlet superconductor. Another way to account for this behavior is to postulate a highly anisotropic energy gap.[5] However, a theoretical study[7] of the energy gap in lead, exploiting the known phonon spectrum and Fermi surface, predicts a gap anisotropy of about ten percent, which is far too small to explain the experimental result. It is important to appreciate that the specific-heat deviation from the Bardeen-Cooper-Schrieffer (BCS) theory cannot be attributed to an incorrect subtraction of the phonon contribution, since the expected BCS result was obtained[5] for $PbIn_{0.06}$. The reversion to a pure exponential law in this latter case also confirms the anisotropic energy-gap interpretation[4,5] since gap anisotropy is washed out by impurity scattering.[8] A dramatic gap anisotropy is also required by the observed low-temperature tail in ultrasonic attenuation.

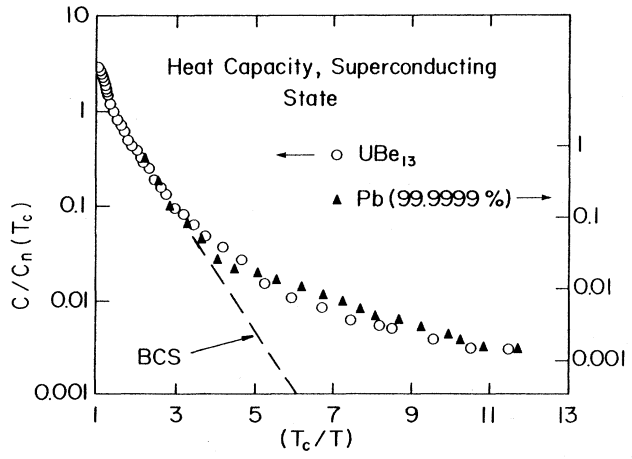

FIG. 1. Electronic specific heat in the superconducting state for Pb and UBe_{13}. The dashed line is the behavior expected from the BCS theory with no (or little) gap anisotropy.

In Sec. II, the most important results regarding spiral and linear SDW's that will be needed in subsequent sections are summarized. Sections III and IV investigate (in turn) superconductivity in the presence of a spiral or a linear SDW for the simplest "metal" of all: jellium. The electron-phonon scattering matrix element is calculated and the BCS gap equation is solved exactly. The critical temperature is determined, together with the effective value of the electron-phonon coupling constant λ. Finally, the specific heat is evaluated numerically as well as the ultrasonic attenuation coefficient. The latter phenomenon also exhibits an important low-temperature deviation from BCS behavior and has been observed by several workers.[9,10] A preliminary report[11] of some of our results has been presented.

II. SPIN-DENSITY WAVES

Before proceeding directly to the study of superconductivity in the presence of a SDW, we shall briefly review the SDW formalism to establish our notations and to focus attention on the most relevant features.

Consider a three-dimensional electron gas with short-range repulsive interactions. The normal state of such a system can be described by a Slater determinant of plane waves within the Hartree-Fock approximation. This state, however, does not necessarily correspond to the

lowest ground-state energy. In fact, Overhauser[12,13] showed that other (exact) solutions of the Hartree-Fock equations can have a lower energy. We now examine in some detail those solutions.

A. Spiral SDW

In this case, the one-electron Hamiltonian can be taken to be

$$H=p^2/2m-G(\sigma_x\cos Qz+\sigma_y\sin Qz)\ , \tag{1}$$

where σ_x, σ_y, and σ_z are the Pauli matrices, and we choose $\mathbf{Q}=2k_F\hat{\mathbf{z}}$. It is a rather simple exercise to find the exact eigenfunctions and eigenvalues of this Hamiltonian. They are,[12] for a (mostly) up-spin state,

$$\phi_{\mathbf{k}\uparrow}(\mathbf{r})=\cos\theta_{\mathbf{k}}\exp(i\mathbf{k}\cdot\mathbf{r})\alpha+\sin\theta_{\mathbf{k}}\exp[i(\mathbf{k}+\mathbf{Q})\cdot\mathbf{r}]\beta\ , \tag{2}$$

where α and β are the usual Pauli spinors. The coefficients are

$$\sin\theta_{\mathbf{k}}=\frac{(\hbar^2k^2/2m)-\varepsilon_{\mathbf{k}}}{\{G^2+[\varepsilon_{\mathbf{k}}-(\hbar^2k^2/2m)]^2\}^{1/2}}\ , \tag{3}$$

$$\cos\theta_{\mathbf{k}}=\frac{G}{\{G^2+[\varepsilon_{\mathbf{k}}-(\hbar^2k^2/2m)]^2\}^{1/2}}\ . \tag{4}$$

The eigenvalues are

$$\varepsilon_{\mathbf{k}}=\frac{\hbar^2}{4m}\left\{k^2+|\mathbf{k}-\mathbf{Q}|^2-\left[(k^2-|\mathbf{k}+\mathbf{Q}|)^2+\left[\frac{4mG}{\hbar^2}\right]^2\right]^{1/2}\right\}. \tag{5}$$

The spin-"up" Fermi surface is shown in Fig. 2(a) and is flattened by an energy gap $2G$ at $k_z=-Q/2$.

For a (mostly) down spin state,

$$\phi_{\mathbf{k}\downarrow}(\mathbf{r})=\cos\theta_{\mathbf{k}}\exp(i\mathbf{k}\cdot\mathbf{r})\beta+\sin\theta_{\mathbf{k}}\exp[i(\mathbf{k}-\mathbf{Q})\cdot\mathbf{r}]\alpha\ , \tag{6}$$

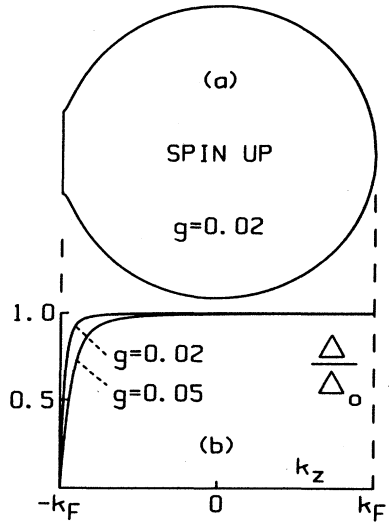

FIG. 2. (a) Fermi surface for the spin-up electrons of a metal having a spiral SDW. (b) Anisotropy of the superconducting gap parameter, $\Delta(k_z)$, for a spiral SDW.

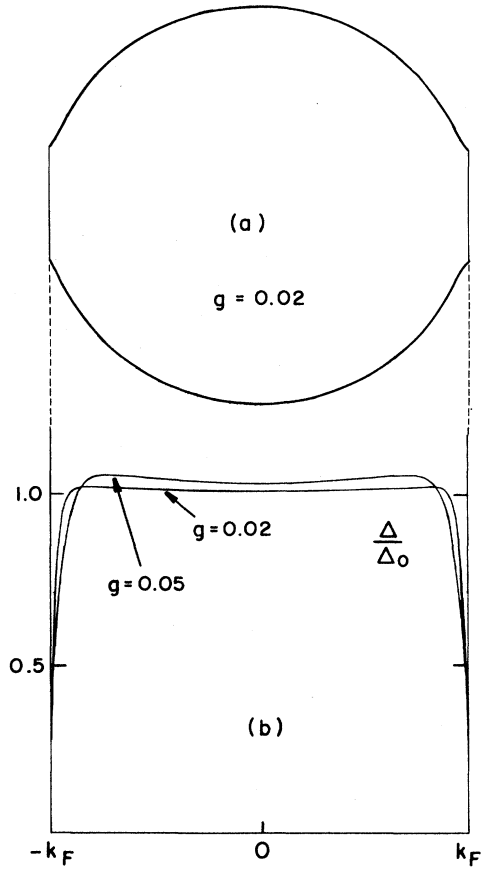

FIG. 3. (a) Fermi surface for the spin-up or spin-down electrons of a metal having a linear SDW. (b) Anisotropy of the superconducting gap parameter, $\Delta(k_z)$, for a linear SDW.

where the coefficients are still given by Eqs. (3) and (4) but $\mathbf{Q}$ has to be replaced by $-\mathbf{Q}$ in Eq. (5). The spin-"down" Fermi surface is similar to the spin-"up" Fermi surface except that it is flattened at $k_z=Q/2$.

In Sec. III the state $\phi_{\mathbf{k}\uparrow}$ will be paired with its *degenerate* partner:

$$\phi_{-\mathbf{k}\downarrow}(\mathbf{r})=\cos\theta_{\mathbf{k}}\exp(-i\mathbf{k}\cdot\mathbf{r})\beta+\sin\theta_{\mathbf{k}}\exp[-i(\mathbf{k}+\mathbf{Q})\cdot\mathbf{r}]\alpha\ , \tag{7}$$

which is not the time reverse of Eq. (2). The time reverse of Eq. (2) would have an opposite sign for the second term in Eq. (7), and would have a higher energy (by $2G$ for states near the SDW gap). Observe that the Hamiltonian [Eq. (1)] does not have time-reversal symmetry. In Eq. (7), the coefficients and $\varepsilon_{\mathbf{k}}$ are given by Eqs. (3)–(5).

B. Linear SDW

The one-electron Hamiltonian for a linear SDW can be taken to be

$$H=\frac{p^2}{2m}-2G\sigma_z\cos Qz\ . \tag{8}$$

For small values of G, the solutions may be approximated

by a linear combination of two plane waves[14]

$$\phi_{\mathbf{k}\uparrow}(\mathbf{r}) \simeq \{\cos\theta_{\mathbf{k}} \exp(i\mathbf{k}\cdot\mathbf{r}) + \sin\theta_{\mathbf{k}} \exp[i(\mathbf{k}+\mathbf{Q})\cdot\mathbf{r}]\}\alpha \ , \quad (9)$$

$$\phi_{\mathbf{k}\downarrow}(\mathbf{r}) \simeq \{\cos\theta_{\mathbf{k}} \exp(i\mathbf{k}\cdot\mathbf{r}) - \sin\theta_{\mathbf{k}} \exp[i(\mathbf{k}+\mathbf{Q})\cdot\mathbf{r}]\}\beta \ , \quad (10)$$

where $-Q/2 < k_z < 0$. The coefficients are still given by Eqs. (3) and (4). The solutions for $0 < k_z < Q/2$ are obtained by replacing $\mathbf{Q}$ with $-\mathbf{Q}$ in Eqs. (9), (10), and (5). The Fermi surface is shown in Fig. 3(a).

III. SUPERCONDUCTIVITY WITH A SPIRAL SDW

A. Electron-phonon interaction

As mentioned previously, the simple "jellium model" will be used to investigate the influence of a spin-density wave on the electron-phonon interaction. It has long been known that, for this model, the Hamiltonian for the phonon mediated electron-electron (*e-e*) interaction is given by[15]

$$H_{e\text{-}e} = \sum_{\mathbf{q}} \sum_{K} \sum_{K'} D_{KK';-\mathbf{q}} D_{\bar{K}\bar{K}';\mathbf{q}} \frac{\hbar\omega_{\mathbf{q}}}{(\varepsilon_K - \varepsilon_{K'})^2 - (\hbar\omega_{\mathbf{q}})^2} \times c^{\dagger}_{\bar{K}'} c_{\bar{K}} c^{\dagger}_{K'} c_K \ , \quad (11)$$

where K (K') designates the initial (final) state—i.e., before (after) exchange of a virtual phonon—and $\bar{K}$ ($\bar{K}'$) is its degenerate partner. $D_{KK';\mathbf{q}}$ has the following simple form:

$$D_{KK';\mathbf{q}} = \tfrac{2}{3} E_F \left[\frac{\hbar q^2}{2NM\omega_{\mathbf{q}}}\right]^{1/2} \int d^3r \phi^{\dagger}_{K'}(\mathbf{r}) \phi_K(\mathbf{r}) \exp(i\mathbf{q}\cdot\mathbf{r}) \ , \quad (12)$$

where M is the ionic mass, N the number of ions per unit volume, and E_F the Fermi energy.

Equations (11) and (12) are, so far, completely general; only pairing between a state and its degenerate partner has been assumed. The final step consists in evaluating $D_{KK';\mathbf{q}}$; this will be done now for a spiral SDW, whereas the linear SDW case will be treated in Sec. IV.

On account of the spin admixture in Eqs. (2) and (7), two terms contribute to Eq. (11). The first one, a "direct" term, is such that both the initial and final states (K and K') are "mostly up" states, i.e., of the form given by Eq. (2). Of course, their degenerate partners are both "mostly down" states. Substitution of Eq. (2) in Eq. (12) leads to

$$D^{\text{direct}}_{\mathbf{k}\mathbf{k}';-\mathbf{q}} = \tfrac{2}{3} E_F \left[\frac{\hbar q^2}{2NM\omega_{\mathbf{q}}}\right]^{1/2} (\cos\theta_{\mathbf{k}}\cos\theta_{\mathbf{k}'} + \sin\theta_{\mathbf{k}}\sin\theta_{\mathbf{k}'}) \times \delta(\mathbf{k}-\mathbf{k}'-\mathbf{q}) \ . \quad (13)$$

The second one, which will become an "exchange term," is such that the initial state $\mathbf{k}$ is, for instance, a "mostly up" state, while the final state $\mathbf{k}'$ is "mostly down." Upon substituting Eqs. (2) and (7) into Eq. (12), one obtains

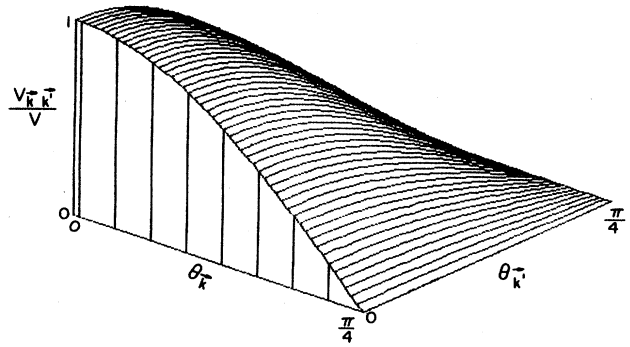

FIG. 4. Virtual-scattering matrix element $V_{\mathbf{k},\mathbf{k}'}$ for a spiral SDW.

$$D^{\text{exchange}}_{\mathbf{k}\mathbf{k}';-\mathbf{q}} = \tfrac{2}{3} E_F \left[\frac{\hbar q^2}{2NM\omega_{\mathbf{q}}}\right]^{1/2} (\sin\theta_{\mathbf{k}}\cos\theta_{\mathbf{k}'} + \cos\theta_{\mathbf{k}}\sin\theta_{\mathbf{k}'}) \times \delta(\mathbf{k}+\mathbf{k}'+\mathbf{Q}-\mathbf{q}) \ . \quad (14)$$

The summation over $\mathbf{q}$ in Eq. (11) can now be performed. After some trivial algebraic manipulations, the Hamiltonian, Eq. (11), can be rewritten:

$$H_{e\text{-}e} = \sum_{\mathbf{k}} \sum_{\mathbf{k}'} V_{\mathbf{k}\mathbf{k}'} c^{\dagger}_{-\mathbf{k}'\downarrow} c_{-\mathbf{k}\downarrow} c^{\dagger}_{\mathbf{k}'\uparrow} c_{\mathbf{k}\uparrow} \ , \quad (15)$$

where

$$V_{\mathbf{k}\mathbf{k}'} = -V \cos 2\theta_{\mathbf{k}} \cos 2\theta_{\mathbf{k}'} \ , \quad (16)$$

and where the $\mathbf{q}$-dependent coefficients have been approximated by a constant (as in the BCS theory) and have been collected in the constant V. As usual, $V_{\mathbf{k}\mathbf{k}'}$ is different from zero only when $\mathbf{k}$ and $\mathbf{k}'$ lie in a thin shell of thickness $2\hbar\omega_D$ centered on the Fermi surface. The matrix element $V_{\mathbf{k},\mathbf{k}'}$, Eq. (16), is shown in Fig. 4 versus the angles $\theta_{\mathbf{k}}$ and $\theta_{\mathbf{k}'}$.

B. Solution of the BCS gap equation

The remarkable fact that $V_{\mathbf{k}\mathbf{k}'}$ appears in factorized form makes it easy to solve the BCS gap equation analytically:[8,16]

$$\Delta(\mathbf{k},T) = \sum_{\mathbf{k}'} V_{\mathbf{k}\mathbf{k}'} \frac{\Delta(\mathbf{k}',T)}{2[\xi^2_{\mathbf{k}'} + \Delta^2(\mathbf{k}',T)]^{1/2}} \times \tanh\left[\frac{[\xi^2_{\mathbf{k}'} + \Delta^2(\mathbf{k}',T)]^{1/2}}{2k_B T}\right] , \quad (17)$$

where $\xi_{\mathbf{k}}$ is the single-particle energy $\varepsilon_{\mathbf{k}}$ measured, however, with respect to the Fermi energy. One can readily verify that

$$\Delta(\mathbf{k},T) = \Delta_0(T)\cos 2\theta_{\mathbf{k}} \quad (18)$$

is the solution of Eq. (17). $\Delta_0(T)$ is a function of temperature only, and it is the solution of the following equation, obtained by substituting Eq. (18) into Eq. (17):

$$1=V\sum_{\mathbf{k}}\cos^2 2\theta_{\mathbf{k}}\frac{\tanh\{[\xi_{\mathbf{k}}^2+\Delta_0^2(T)\cos^2 2\theta_{\mathbf{k}}]^{1/2}/2k_BT\}}{2[\xi_{\mathbf{k}}^2+\Delta_0^2(T)\cos^2 2\theta_{\mathbf{k}}]^{1/2}} . \tag{19}$$

$\Delta_0(T)$ varies with temperature in a way similar to the isotropic gap parameter in BCS theory.

Since $\theta_{\mathbf{k}}=\pi/4$ at the SDW gap, as can be seen from Eq. (3), Δ vanishes at the SDW gap. The Fermi-surface neck, shown in Fig. 2(a) and caused by the SDW, has in general a finite circumference. Accordingly, the superconducting gap Δ has a line of nodes on the Fermi surface. This feature leads automatically to a power-law tail in the low-temperature specific heat (Sec. III D). The reduced gap $\Delta(\mathbf{k},T)/\Delta_0(T)$ is shown in Fig. 2(b) for different values of the dimensionless parameter

$$g\equiv\frac{G}{4E_F} . \tag{20}$$

It is important to notice that although the anisotropy of Δ is enormous, it is confined to a small fraction of the Fermi surface near the SDW gap. For simplicity we choose to keep $\mathbf{Q}=2k_F\hat{\mathbf{z}}$ independent of g, so that the density of states at the Fermi surface (a quantity measured experimentally) remains the same for all values of g. Consequently, the Fermi energy depends weakly on g.

C. Critical temperature

At T_c the gap Δ vanishes. This provides us with the following equation for T_c:

$$1=V\sum_{\mathbf{k}}\cos^2 2\theta_{\mathbf{k}}\frac{\tanh(\xi_{\mathbf{k}}/2k_BT)}{2\xi_{\mathbf{k}}} , \tag{21}$$

where the summation extends over all $\mathbf{k}$ vectors lying in a shell of thickness $2\hbar\omega_D$ centered on the Fermi surface, as shown in Fig. 5. In the weak-coupling (BCS) limit, Eq. (21) can be solved exactly; to this end, the sum over $\mathbf{k}$ is first replaced by an integral. On account of the cylindrical symmetry of the Fermi surface, this integral is most easily evaluated in cylindrical coordinates. So, with the notations of Fig. 5, Eq. (21) becomes

$$1=\frac{V}{4\pi^2}\left[\int_{-k_F}^{k_+}dk_z\int_0^{K_+(k_z)}dk_\perp k_\perp\cos^2 2\theta_{\mathbf{k}}\frac{\tanh(\xi_{\mathbf{k}}/2k_BT)}{2\xi_{\mathbf{k}}}-\int_{-k_F}^{k_-}dk_z\int_0^{K_-(k_z)}dk_\perp k_\perp\cos^2 2\theta_{\mathbf{k}}\frac{\tanh(\xi_{\mathbf{k}}/2k_BT)}{2\xi_{\mathbf{k}}}\right] . \tag{22}$$

Now, it follows from Eq. (5) that $\xi_{\mathbf{k}}$ is of the form

$$\xi_{\mathbf{k}}=\frac{\hbar^2k_\perp^2}{2m}+\alpha(k_z) , \tag{23}$$

where $\alpha(k_z)$ depends on k_z only. Furthermore, let

$$k'_z=k_z+k_F . \tag{24}$$

Equations (23) and (24) together form a two-dimensional change of variables, the Jacobian of which is readily evaluated [notice that an explicit expression for $\alpha(k_z)$ is not needed]. Equation (22) becomes

$$1=\frac{V}{8\pi^2}\frac{m}{\hbar^2}\int_0^{2k_F}dk_z\cos 2\theta_{k_z}\int_{-\hbar\omega_D}^{\hbar\omega_D}d\xi\frac{\tanh(\xi/2k_BT)}{\xi} . \tag{25}$$

To obtain this result, it has further been assumed that, owing to the smallness of $\hbar\omega_D$, it follows that $k_+,k_-\approx k_F$. We have also made explicit the fact that

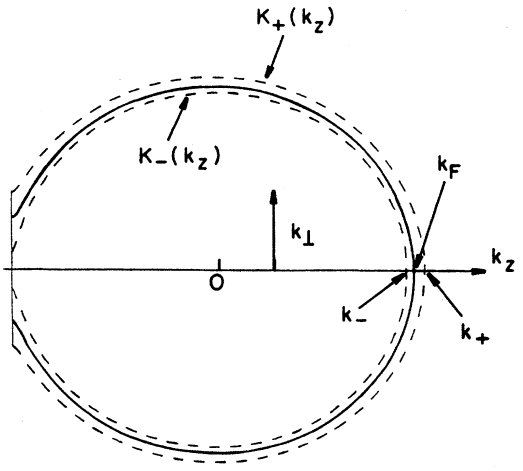

FIG. 5. Notations for Eq. (22).

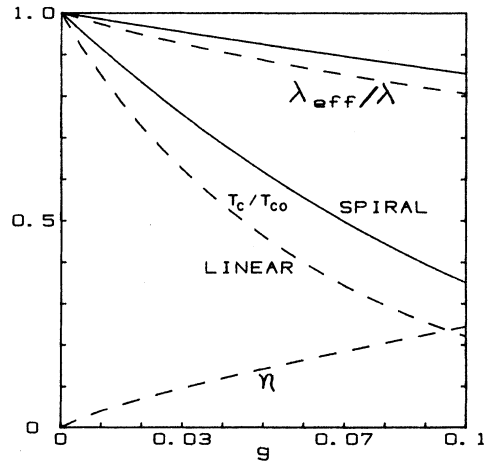

FIG. 6. g dependence [see Eq. (20)] of λ_{eff} and T_c (from McMillan's equation with $\lambda=0.4$ and $\mu^*=0.1$). $\eta\Delta_0(T)$ is the superconducting gap parameter at the (linear) SDW gap. ($\eta\equiv 0$ for the spiral case).

$\cos 2\theta_{\mathbf{k}}$ depends only on k_z, which can be inferred from Eqs. (3)–(5). The right-hand side of Eq. (25) is now the product of one-dimensional integrals. Upon replacing $\cos 2\theta_{k_z}$ by its expression in terms of k_z, the first integral can be calculated analytically, while the second one is a well-known integral in BCS theory. It can be evaluated easily in the weak-coupling limit. After some tedious, but simple, algebra, one gets the usual BCS expression for T_c

$$k_B T_c = 1.14\hbar\omega_D \exp(-1/\lambda_{\text{eff}}) , \tag{26}$$

but with

$$\lambda_{\text{eff}} = \lambda[1 - g \arctan(1/g)] . \tag{27}$$

It is interesting to substitute λ_{eff} for λ in McMillan's equation[17] for T_c. Both λ_{eff} and T_c versus g are shown in Fig. 6. Superconductivity is quenched by a large SDW gap. Notice also that in the large g limit, one recovers the ferromagnetic limit, i.e., λ_{eff} goes to zero (as does T_c).

D. Electronic specific heat

We now consider the effects of anisotropy on the electronic specific heat, c_{es}, and its low-temperature behavior. c_{es} is given by[18]

$$c_{\text{es}} = \frac{2}{k_B T^2} \sum_{\mathbf{k}} f_{\mathbf{k}}(1-f_{\mathbf{k}}) \left[\xi_{\mathbf{k}}^2 + \Delta^2(\mathbf{k},T) - T\Delta(\mathbf{k},T)\frac{\partial\Delta(\mathbf{k},T)}{\partial T} \right] , \tag{28}$$

where

$$f_{\mathbf{k}} = \frac{1}{1+\exp\{[\xi_{\mathbf{k}}^2+\Delta^2(\mathbf{k},T)]^{1/2}/k_B T\}} ,$$

is the Fermi-Dirac distribution for quasiparticles.

We calculated the specific heat by numerical evaluation of Eq. (28) for several values of g. The results are shown in Fig. 7. A rather intricate calculation, detailed in Appendix A, shows that close to absolute zero the specific heat has the following asymptotic behavior:

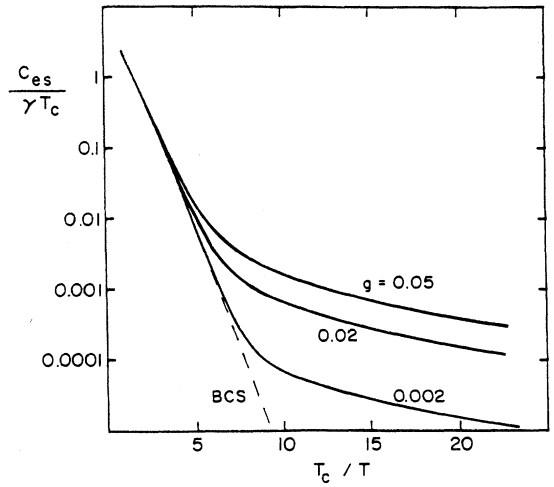

FIG. 7. Electronic specific heat in the superconducting state vs T_c/T for a spiral SDW. SDW gap parameter g is defined by Eq. (20).

$$c_{\text{es}}(T) \sim \frac{105}{8} \frac{m k_F g k_B^3}{\pi^2 \hbar^2 \Delta_0} T^2 , \tag{29}$$

where $\Delta_0 = \Delta_0(0)$. This power-law behavior is caused, as already mentioned, by the line of nodes at the Fermi surface.

IV. SUPERCONDUCTIVITY WITH A LINEAR SDW

A. Electron-phonon interaction

The calculation of the virtual-scattering matrix element for the linear SDW case is straightforward. Both initial and final states correspond to a well-defined spin state and no exchange term appears, as in the spiral SDW case. Substitution of Eq. (9) into Eq. (12) leads to

$$D_{\mathbf{k},\mathbf{k}';-\mathbf{q}} = \tfrac{2}{3}E_F \left[\frac{\hbar q^2}{2NM\omega_{\mathbf{q}}} \right]^{1/2} [\cos(\theta_{\mathbf{k}}-\theta_{\mathbf{k}'})\delta(\mathbf{k}-\mathbf{k}'-\mathbf{q}) + \sin\theta_{\mathbf{k}}\cos\theta_{\mathbf{k}'}\delta(\mathbf{k}-\mathbf{k}'-\mathbf{q}+\mathbf{Q}) + \cos\theta_{\mathbf{k}}\sin\theta_{\mathbf{k}'}\delta(\mathbf{k}-\mathbf{k}'-\mathbf{q}-\mathbf{Q})] . \tag{30}$$

It is clear from Eq. (30) that coupling can occur through virtual emission of phonons $\mathbf{q}$, $\mathbf{q}+\mathbf{Q}$, and $\mathbf{q}-\mathbf{Q}$, a consequence of the nature of the SDW one-particle wave functions, Eqs. (9) and (10). Upon adoption of the simplifications already described in Sec. III, it is easy to show that the virtual-scattering matrix element $V_{\mathbf{k}\mathbf{k}'}$ is given by

$$V_{\mathbf{k}\mathbf{k}'} = -V(\cos 2\theta_{\mathbf{k}}\cos 2\theta_{\mathbf{k}'} + \tfrac{1}{2}\sin 2\theta_{\mathbf{k}}\sin 2\theta_{\mathbf{k}'}) . \tag{31}$$

This $\mathbf{k}$ dependence is shown in Fig. 8.

B. Solution of the gap equation

Since $V_{\mathbf{k}\mathbf{k}'}$ does not appear in factorized form, the Markowitz-Kadanoff theory[8,16] can no longer be used. However, $V_{\mathbf{k}\mathbf{k}'}$ is a sum of factorized terms, and a treatment similar to that for linear Fredholm integral equations with degenerate kernel can be applied to the BCS integral equation.[19] For notational convenience, we define

$g_{\mathbf{k}}=\cos 2\theta_{\mathbf{k}}$,

$h_{\mathbf{k}}=\sin 2\theta_{\mathbf{k}}$.

Using Eq. (31), we first rewrite the BCS integral equation in the following way:

$$\Delta(\mathbf{k},T)=Vg_{\mathbf{k}}\sum_{\mathbf{k}'}g_{\mathbf{k}'}\frac{\tanh\{[\xi_{\mathbf{k}'}^2+\Delta^2(\mathbf{k}',T)]^{1/2}/2k_BT\}}{2[\xi_{\mathbf{k}'}^2+\Delta^2(\mathbf{k}',T)]^{1/2}}\Delta(\mathbf{k}',T)+\tfrac{1}{2}Vh_{\mathbf{k}}\sum_{\mathbf{k}'}h_{\mathbf{k}'}\frac{\tanh\{[\xi_{\mathbf{k}'}^2+\Delta^2(\mathbf{k}',T)]^{1/2}/2k_BT\}}{2[\xi_{\mathbf{k}'}^2+\Delta^2(\mathbf{k}',T)]^{1/2}}\Delta(\mathbf{k}',T)\ . \tag{32}$$

This suggests a solution of the form

$$\Delta(\mathbf{k},T)=V[c_1(T)g_{\mathbf{k}}+c_2(T)h_{\mathbf{k}}]\ , \tag{33}$$

where $c_1(T)$ and $c_2(T)$ are temperature-dependent constants to be determined. Substituting Eq. (33) in Eq. (32), and recognizing that $g_{\mathbf{k}}$ and $h_{\mathbf{k}}$ are linearly independent, one obtains the following two equations for c_1 and c_2:

$$c_1-\sum_{\mathbf{k}}Vg_{\mathbf{k}}(c_1g_{\mathbf{k}}+c_2h_{\mathbf{k}})\frac{\tanh\{[\xi_{\mathbf{k}}^2+V^2(c_1g_{\mathbf{k}}+c_2h_{\mathbf{k}})^2]^{1/2}/2k_BT\}}{2[\xi_{\mathbf{k}}^2+V^2(c_1g_{\mathbf{k}}+c_2h_{\mathbf{k}})^2]^{1/2}}=0\ , \tag{34}$$

$$c_2-\tfrac{1}{2}\sum_{\mathbf{k}}Vh_{\mathbf{k}}(c_1g_{\mathbf{k}}+c_2h_{\mathbf{k}})\frac{\tanh\{[\xi_{\mathbf{k}}^2+V^2(c_1g_{\mathbf{k}}+c_2h_{\mathbf{k}})^2]^{1/2}/2k_BT\}}{2[\xi_{\mathbf{k}}^2+V^2(c_1g_{\mathbf{k}}+c_2h_{\mathbf{k}})^2]^{1/2}}=0\ . \tag{35}$$

Equations (34) and (35) form a set of two nonlinear, algebraic equations, the solution of which completely determines the superconducting gap. At this point, it is convenient to introduce two new functions $\Delta_0(T)$ and $\eta(T)$ instead of $c_1(T)$ and $c_2(T)$:

$\Delta_0(T)\equiv c_1(T)V$,

$\eta(T)\equiv\dfrac{c_2(T)}{c_1(T)}V$.

The superconducting gap can now be rewritten in terms of $\Delta_0(T)$ and $\eta(T)$:

$$\Delta(\mathbf{k},T)=\Delta_0(T)[\cos 2\theta_{\mathbf{k}}+\eta(T)\sin 2\theta_{\mathbf{k}}]\ , \tag{36}$$

as well as Eqs. (34) and (35):

$$1-\sum_{\mathbf{k}}Vg_{\mathbf{k}}[g_{\mathbf{k}}+\eta(T)h_{\mathbf{k}}]\frac{\tanh\{[\xi_{\mathbf{k}}^2+\Delta_0^2(T)(g_{\mathbf{k}}+\eta(T)h_{\mathbf{k}})^2]^{1/2}/2k_BT\}}{2[\xi_{\mathbf{k}}^2+\Delta_0^2(T)(g_{\mathbf{k}}+\eta(T)h_{\mathbf{k}})^2]^{1/2}}=0\ , \tag{37}$$

$$1-\tfrac{1}{2}\sum_{\mathbf{k}}Vh_{\mathbf{k}}[g_{\mathbf{k}}/\eta(T)+h_{\mathbf{k}}]\frac{\tanh\{[\xi_{\mathbf{k}}^2+\Delta_0^2(T)(g_{\mathbf{k}}+\eta(T)h_{\mathbf{k}})^2]^{1/2}/2k_BT\}}{2[\xi_{\mathbf{k}}^2+\Delta_0^2(T)(g_{\mathbf{k}}+\eta(T)h_{\mathbf{k}})^2]^{1/2}}=0\ . \tag{38}$$

In general, this set of equations has to be solved numerically. This task, however, is not as formidable as it might look at first sight. Indeed, it is shown in Appendix B that $\eta(T)$ is in fact temperature independent and can even be determined analytically (see Sec. IV C). This considerably simplifies the resolution of Eqs. (37) and (38) since only one of them has to be solved once η is known. The gap is shown in Fig. 3(b) for several values of g. Notice that the gap no longer vanishes at the SDW gap, as in the spiral SDW case, but rather falls to a small value, $\eta\Delta_0$. This will lead to a low temperature dependence of the electronic specific heat somewhat different from that obtained for a spiral SDW.

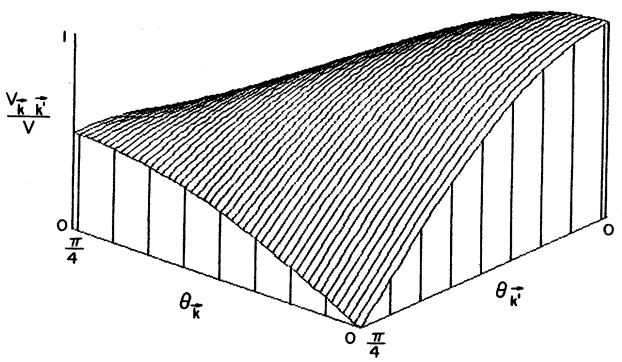

FIG. 8. Virtual-scattering matrix element $V_{\mathbf{k},\mathbf{k}'}$ for a linear SDW.

C. Critical temperature

At T_c, the gap $\Delta(\mathbf{k},T)$, or more precisely Δ_0, vanishes. Hence, from Eq. (37), we obtain the following relation-

ship between η and T_c:

$$1-\sum_{\mathbf{k}} V g_{\mathbf{k}}(g_{\mathbf{k}}+\eta h_{\mathbf{k}})\frac{\tanh(\xi_{\mathbf{k}}/2k_BT)}{2\xi_{\mathbf{k}}}=0\ , \tag{39}$$

while from Eq. (38) one gets

$$1-\tfrac{1}{2}\sum_{\mathbf{k}} V h_{\mathbf{k}}(g_{\mathbf{k}}/\eta+h_{\mathbf{k}})\frac{\tanh(\xi_{\mathbf{k}}/2k_BT)}{2\xi_{\mathbf{k}}}=0\ . \tag{40}$$

These two equations can be solved exactly in the weak-coupling limit. To this end, we first replace the summation over $\mathbf{k}$ by an integral in cylindrical coordinates, according to the symmetry of the Fermi surface. The following steps will be performed on Eq. (39) only. [The calculations for Eq. (40) are similar, and we will merely quote the final result.] With the notations of Fig. 9, Eq. (39) becomes

$$1-\frac{V}{2\pi^2}\int_0^{k_F}dk_z\int_{K_-(k_z)}^{K_+(k_z)}dk_\perp k_\perp g_{\mathbf{k}}(g_{\mathbf{k}}+\eta h_{\mathbf{k}})\times\frac{\tanh(\xi_{\mathbf{k}}/2k_BT)}{2\xi_{\mathbf{k}}}=0\ . \tag{41}$$

Next, we perform a change of variables, Eq. (23), followed by the change of variables Eqs. (52) and (53), displayed in Appendix A. The final result is

$$1-2\lambda g\int_0^{\operatorname{arcsinh}(1/2g)}dt\,\tanh t(\sinh t+\eta)\times\int_0^{\hbar\omega_D/2k_BT_c}du\frac{\tanh u}{u}=0\ . \tag{42}$$

A similar calculation for Eq. (40) leads to

$$1-2\lambda_g\int_0^{\operatorname{arcsinh}(1/2g)}dt\frac{\sinh t+\eta}{2\eta\cosh t}\times\int_0^{(\hbar\omega_D/2k_BT_c)}du\frac{\tanh u}{u}=0\ . \tag{43}$$

At this point, it is clear that η can easily be eliminated between Eqs. (42) and (43):

$$\eta=\frac{1-2\lambda gF\int_0^{\operatorname{arcsinh}(1/2g)}dt(\sinh^2 t/\cosh t)}{2\lambda gF\int_0^{\operatorname{arcsinh}(1/2g)}dt\tanh t}=\frac{\lambda gF\int_0^{\operatorname{arcsinh}(1/2g)}dt\tanh t}{1-\lambda gF\int_0^{\operatorname{arcsinh}(1/2g)}dt(1/\cosh t)}\ , \tag{44}$$

where F depends essentially on T_c and is defined by

$$F=\int_0^{\hbar\omega D/2k_BT_c}du\frac{\tanh u}{u}\ . \tag{45}$$

This expression can be evaluated in the weak-coupling limit and leads to the well-known result[13]

$$F=\ln\left[1.14\frac{\hbar\omega_D}{k_BT_c}\right]\ . \tag{46}$$

All of the integrals appearing in Eq. (44) can be evaluated analytically and Eq. (44) reduces to a quadratic equation for F, from which T_c can be extracted:

$$k_BT_c=1.14\hbar\omega_D\exp(-1/\lambda_{\text{eff}})\ . \tag{47}$$

λ_{eff} is given by

$$\lambda_{\text{eff}}=\tfrac{1}{2}\lambda\{1-v+[(1-3v)^2+2u^2]^{1/2}\}\ , \tag{48}$$

where $u\equiv g\ln(1+1/4g^2)$ and $v\equiv g\arctan(1/2g)$.

Substituting these results in Eq. (44), one obtains an exact value for η,

$$\eta=\frac{u}{2[(\lambda_{\text{eff}}/\lambda)-v]}\ . \tag{49}$$

λ_{eff}, T_c, and η versus g are shown in Fig. 6. Again McMillan's equation with λ replaced by λ_{eff} has been used rather than the BCS-like formula, Eq. (47).

D. Electronic specific heat

We have calculated the electronic specific heat by the numerical evaluation of Eq. (28). The results are shown in Fig. 10 for several values of g. The low-temperature

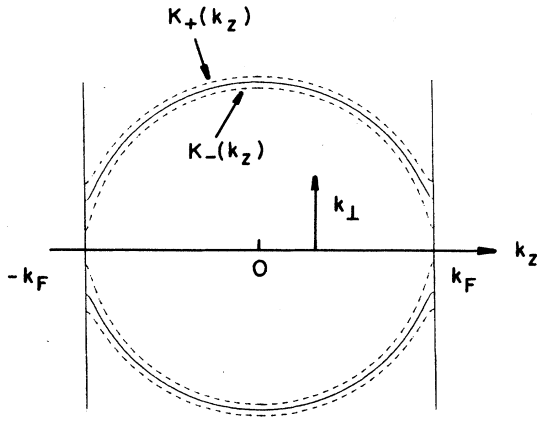

FIG. 9. Notations for Eq. (40).

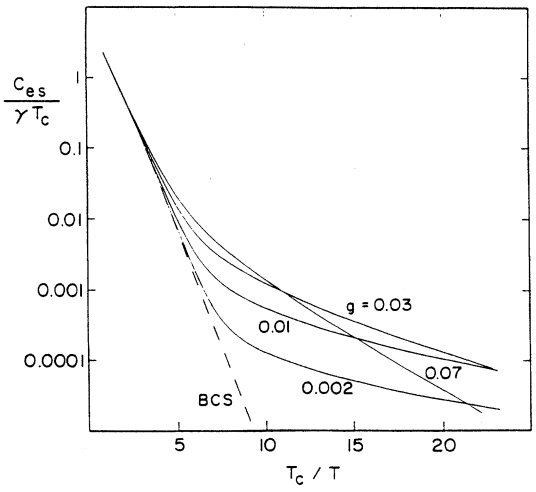

FIG. 10. Electronic specific heat in the superconducting state vs T_c/T for a linear SDW.

behavior is no longer a power law as for the case of a spiral SDW. This arises from the fact that the superconducting gap no longer vanishes at $\pm\mathbf{Q}/2$, but rather falls to a small value $\eta\Delta_0$ as already mentioned. Now as g increases, η increases, thereby reducing the gap anisotropy when g is large enough. This behavior causes the low-temperature specific heat to revert to a BCS-like exponential falloff, but to one having a much smaller slope than ideal BCS behavior.

E. Ultrasonic attenuation

Finally, we examine how the gap anisotropy caused by a linear SDW affects the ultrasonic attenuation. A "long tail," similar to that of the specific-heat curve, appears at low temperature. This is reminiscent of the experimental results obtained in Pb by Fate, Shaw, and Salinger[9] and also by Randorff and Marshall.[10] (See also Ref. 20 and references therein for a recent discussion of the experimental situation.) Shown in Fig. 11 is the experimental curve obtained by Fate *et al.*,[9] juxtaposed with the expected behavior from the BCS theory. Besides the presence of this "long tail" at low temperature, the ultrasonic attenuation in Pb exhibits two other anomalies.[9,10,21] Just below T_c the attenuation decreases too rapidly (with decreasing T) compared to the BCS prection. (This causes the attenuation curve in Fig. 11 to rise above the BCS line.) Furthermore, this anomalous dependence near T_c is frequency dependent. So far, such effects have not been explained. In what follows, we shall focus our attention on the low-temperature anomaly.

We employ a simple deformation-potential model[22] to calculate the attenuation coefficient. In order to concentrate on the effect of the superconducting gap anisotropy, we take a spherical Fermi surface, so as to avoid any complexity that might arise from the angle between the propagation direction of the acoustic wave and $\mathbf{Q}$. The ratio between the ultrasonic attenuation coefficient in the superconducting state, α_S, and that in the normal state, α_N is

$$\frac{\alpha_S}{\alpha_N}=-\frac{1}{N(0)}\sum_{\mathbf{k}}\frac{\xi_{\mathbf{k}}}{E_{\mathbf{k}}}\frac{\partial f}{\partial E_{\mathbf{k}}}\,, \tag{50}$$

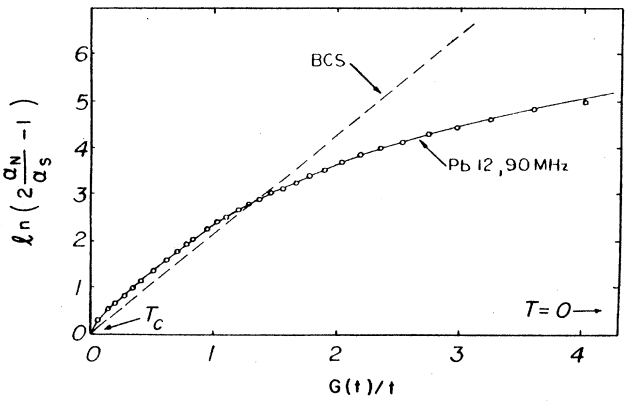

FIG. 11. Experimental ultrasonic attenuation coefficient (from Ref. 18).

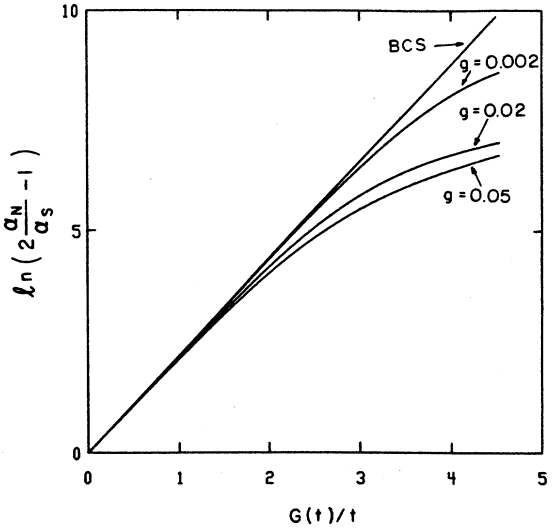

FIG. 12. Ultrasonic attenuation coefficient for a metal having a linear SDW.

where $N(0)$ is the density of states (per spin) at the Fermi surface and $E_{\mathbf{k}}=[\xi_{\mathbf{k}}^2+\Delta(\mathbf{k},T)^2]^{1/2}$. The transformation of this sum into an integral (followed by simple algebra) yields the result shown in Fig. 12 for different values of g. The quantity

$$\ln\left[2\frac{\alpha_N}{\alpha_S}-1\right],$$

is plotted versus

$$\frac{G(t)}{t}\equiv\frac{1}{t}\frac{\Delta(t)}{\Delta_0(0)}\,,$$

where $t\equiv T/T_c$. In such a plot the BCS curve for an isotropic energy gap is just a straight line with slope $\Delta_0(0)/k_BT_c$. Notice the significant deviation of the calculated curves from the BCS straight line at low temperature.

Comparison of Figs. 11 and 12 leads to the conclusion that the SDW structure can account for the low-temperature anomalies observed in Pb for the ultrasonic attenuation as well as for the specific heat. If this were true, we expect that Pb will have a cubic family of small-amplitude, linear SDW's, e.g., $\mathbf{Q}$'s along twelve [211] axes. It is possible to estimate the SDW transition temperature T_{SDW} from the data in Fig. 1. The specific-heat tail (near $T_c/T=11$) caused by each SDW would be about $\frac{1}{12}$ the value shown in Fig. 1, i.e., slightly above the curve for $g=0.002$ in Fig. 10. It follows from Eq. (20) that each SDW gap is $2G\sim0.2$ eV. Since $2G\sim3.5k_BT$,[13] we find $T_{\mathrm{SDW}}\sim660$ K, which is above the melting point. Accordingly we would not anticipate transport anomalies caused by a SDW phase transition in the normal state of (crystalline) Pb.

ACKNOWLEDGMENTS

The authors are grateful to the National Science Foundation, Condensed-Matter Theory Section, for financial support.

APPENDIX A

At low temperature, Δ_0 is essentially constant, and the term proportional to its derivative with respect to T in Eq. (28) can be neglected. In what follows, we let $\Delta_0 \equiv \Delta_0(0)$. Upon replacing the sum over $\mathbf{k}$ in Eq. (28) by an integral and performing the change of variables defined by Eqs. (23) and (24), c_{es} can be written as

$$c_{es}=\frac{m}{\pi^2\hbar^2 k_B T^2}\int_0^{2k_F} dk_z \int_0^{\infty} d\xi[\xi^2+\Delta^2(k_z,T)]\frac{\exp\{[\xi^2+\Delta^2(k_z,T)]^{1/2}/k_B T\}}{1+\exp\{[\xi^2+\Delta^2(k_z,T)]^{1/2}/k_B T\}} . \tag{51}$$

(States for which $k_z < -k_F$ or $k_z > k_F$ give a negligible contribution to c_{es} and have not been included.) By means of successive changes of variables

$$\xi = k_B T u , \tag{52}$$

$$k_z = 2gk_F \sinh t , \tag{53}$$

and by the use of Eqs. (3), (4), and (8), one obtains

$$c_{es}=\frac{2mk_F g k_B^2 T}{\pi^2\hbar^2}\int_0^{\operatorname{arcsinh}(1/g)} dt \cosh t \int_0^{\infty} du \left[u^2+\left[\frac{\Delta_0}{k_B T}\right]^2\right]\frac{\exp[u^2+(\Delta_0/k_B T)^2]}{1+\exp[u^2+(\Delta_0/k_B T)^2]}$$

$$\approx\frac{2mk_F g k_B^2 T}{\pi^2\hbar^2}\int_0^{\operatorname{arcsinh}(1/g)} dt \cosh t \int_0^{\infty} du[u^2+a^2(t)]\exp\{-[u^2+a^2(t)]^{1/2}\} , \tag{54}$$

where $a(t)\equiv\Delta_0 \tanh t/k_B T$.

Let $I(t)$ be the result obtained by performing the integration over u in Eq. (54). Using the change of variable, $u = a(t)\sinh u$, one gets

$$I(t)=\int_0^{\infty} dx\, a^3(t)\cosh^3 x \exp[-a(t)\cosh x]$$

$$=-a^3(t)\frac{\delta^3}{\delta[a(t)]^3}\int_0^{\infty}\exp[-a(t)\cosh x]=a^3(t)\{\tfrac{3}{4}K_1[a(t)]+\tfrac{1}{4}K_3[a(t)]\} , \tag{55}$$

where K_1 and K_3 are modified Bessel functions of the second kind. Subsitution of Eq. (55) into Eq. (54) leads to

$$c_{es}\approx\frac{2mk_F g k_B^2 T}{\pi^2\hbar^2}\left[\frac{\Delta_0}{k_B T}\right]^3\int_0^{\operatorname{arcsinh}(1/g)} dt\frac{\sinh^3 t}{\cosh^2 t}\left[\tfrac{3}{4}K_1\left[\frac{\Delta_0}{k_B T}\tanh t\right]+\tfrac{1}{4}K_3\left[\frac{\Delta_0}{k_B T}\tanh t\right]\right] . \tag{56}$$

At low temperature, it can be seen from the behavior of K_1 and K_3 for large and small arguments[23] that only small values of T contribute significantly to the integral. Near $T=0$, the contribution of K_3 is the most important one; upon taking this into account and performing the change of variable,

$$x=\frac{\Delta_0}{k_B T}\tanh t ,$$

one gets

$$c_{es}\approx\frac{mk_F g\Delta_0^2}{2\pi^2\hbar^2 T}\int_0^{\infty} dx\, K_3(x)\frac{x^3}{[(\Delta_0/k_B T)^2-x^2]^{3/2}} , \tag{57}$$

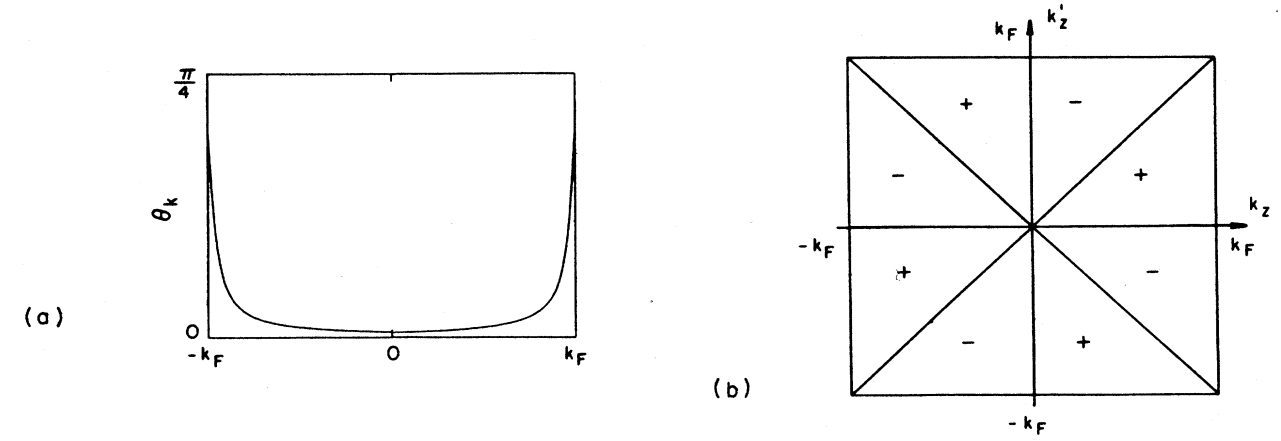

FIG. 13. (a) The angle $\theta_{\mathbf{k}}$ vs k_z. (b) The "summation domain" for Eq. (60). The sign of $\sin(2\theta_{\mathbf{k}}-2\theta_{\mathbf{k}'})$ is indicated.

where the integration has been extended to infinity (a good approximation at low temperature and reasonably small g). Due to the rapid decay at infinity of $K_3(x)$, only small values of x contribute signficantly in Eq. (57), so that finally

$$c_{es} \approx \frac{mk_F g k_B^3 T^2}{2\pi^2 \hbar^2 \Delta_0} \int_0^\infty dx\, x^3 K_3(x) \approx \frac{105}{8} \frac{mk_F g k_B^3}{\pi^2 \hbar^2 \Delta_0} T^2 . \tag{58}$$

APPENDIX B

In this appendix we prove that the parameter η which appears in Eq. (36) is temperature independent. We shall merely sketch the proof; the details of the lengthy (but simple) calculation are left to the reader.

Equations (37) and (38) form a system of two nonlinear equations for $\Delta_0(T)$ and $\eta(T)$; they have the following general form:

$$f(\Delta_0, \eta, T) = 0 ,$$

$$g(\Delta_0, \eta, T) = 0 .$$

From these equations, we extract

$$\frac{d\eta}{dT} = \frac{(\partial f/\partial \Delta_0)(\partial g/\partial T) - (\partial g/\partial \Delta_0)(\partial f/\partial T)}{(\partial f/\partial \Delta_0)(\partial g/\partial \eta) - (\partial g/\partial \Delta_0)(\partial f/\partial \eta)} \equiv \frac{N}{D} . \tag{59}$$

The partial derivatives appearing in Eq. (59) can be evaluated exactly from Eqs. (37) and (38). One finds a result of the form

$$N = \sum_{\mathbf{k}} \sum_{\mathbf{k}'} \alpha_{\mathbf{k}} \beta_{\mathbf{k}'} \sin(2\theta_{\mathbf{k}} - 2\theta_{\mathbf{k}'}) , \tag{60}$$

where the only properties of $\alpha_{\mathbf{k}}$ and $\beta_{\mathbf{k}}$ of interest to us here are

$$\alpha_{-\mathbf{k}} = \alpha_{\mathbf{k}} , \tag{61}$$

$$\beta_{-\mathbf{k}} = \beta_{\mathbf{k}} . \tag{62}$$

The angle $\theta_{\mathbf{k}}$ versus k_z is shown in Fig. 13(a) together with the "summation domain" where the sign of $\sin(2\theta_{\mathbf{k}} - 2\theta_{\mathbf{k}'})$ is indicated [Fig. 13(b)]. So it is obvious that, by symmetry, the sum [Eq. (60)] vanishes; hence, $d\eta/dT = 0$, and η is temperature independent.

[1] W. Baltensperger and S. Strässler, Phys. Kondens. Mater. **1**, 20 (1963).
[2] M. J. Nass, K. Levin, and G. S. Grest, Phys. Rev. Lett. **46**, 614 (1981).
[3] G. C. Psaltakis and E. W. Fenton, J. Phys. C **16**, 3913 (1983).
[4] P. H. Keesom and B. J. C. van der Hoeven, Phys. Lett. **3**, 360 (1963).
[5] B. J. C. van der Hoeven and P. H. Keesom, Phys. Rev. **137**, A103 (1965).
[6] H. R. Ott, H. Rudigier, T. M. Rice, K. Ueda, Z. Fisk, and J. L. Smith, Phys. Rev. Lett. **52**, 1915 (1984).
[7] Alan J. Bennett, Phys. Rev. **140**, A1902 (1965).
[8] D. Markowitz and L. P. Kadanoff, Phys. Rev. **131**, 563 (1963).
[9] W. A. Fate, R. W. Shaw, and G. L. Salinger, Phys. Rev. **172**, 413 (1968).
[10] J. E. Randorff and B. J. Marshall, Phys. Rev. B **2**, 100 (1970).
[11] A. W. Overhauser and L. L. Daemen, Phys. Rev. Lett. **61**, 1885 (1988).
[12] A. W. Overhauser, Phys. Rev. Lett. **4**, 462 (1960).
[13] A. W. Overhauser, Phys. Rev. **128**, 1437 (1962).
[14] A. W. Overhauser, Phys. Rev. Lett. **13**, 190 (1964).
[15] G. Grimvall, *The Electron-Phonon Interaction in Metals* (North-Holland, Amsterdam, 1981).
[16] J. R. Clem, Ann. Phys. (N.Y.) **40**, 268 (1966).
[17] W. L. McMillan, Phys. Rev. **167**, 331 (1968).
[18] P. G. de Gennes, *Superconductivity of Metals and Alloys* (Benjamin, New York, 1966).
[19] S. G. Mikhlin, *Integral Equations* (Pergamon, New York, 1957).
[20] Jacob Philip, B. K. Basu, and K. Samudravijaya, J. Low Temp. Phys. **67**, 453 (1987).
[21] W. A. Fate and R. W. Shaw, Phys. Rev. Lett. **19**, 230 (1967); B. C. Deaton, *ibid.* **16**, 577 (1966); B. K. Basu, Pramana, **22**, 439 (1984).
[22] P. G. de Gennes, *Superconductivity of Metals and Alloys* (Benjamin, New York, 1966), p. 131.
[23] M. Abramowitz and I. E. Stegun, *Handbook of Mathematical Functions* (Dover, New York, 1970).